Performance Evaluation of Dual-Drive Mach-Zehnder Modulator and Optomechanical Crystal Cavity Comb Generation for All-Optical Band Conversion in 5G-Advanced Cellular Systems

Vicente Fito, Raúl Ortiz, Maria Morant, *Member, IEEE*, Laura Mercadé, *Member, IEEE*, Alejandro Martínez, *Senior Member, IEEE*, and Roberto Llorente, *Member, IEEE*

***Abstract*—Multiband operation is a key aspect of emerging 5G-Advanced cellular systems, also named 5.5G, which target seamless provision of multi-gigabit per second connectivity employing sub-6 GHz and mm-wave overlapping coverage. All-optical frequency conversion gives flexibility due to the feasible high-speed reconfiguration in broad bands and large radio signal bandwidth. Optical frequency combs, featuring a spectrum of discrete, equally spaced coherent frequency lines, are crucial for high-precision metrology, spectroscopy, and telecommunications. Their effectiveness in all-optical frequency conversion depends on their stability in terms of frequency drift, phase noise, and power distribution across the comb lines. This paper evaluates experimentally the generation of optical frequency combs employing two distinct technologies: a dual-driven Mach-Zehnder modulator (DD-MZM) and an optomechanical crystal cavity (OMCC), and experimentally compares their performance for all-optical frequency conversion of 5G data streams. The DD-MZM implementation generates a comb with flexible line spacing and comprising several spectrum-flat lines with low phase noise (-88.5 dBc/Hz at 1 kHz offset and -108.3 dBc/Hz at 100 kHz offset). The OMCC implementation provides a reduced footprint (182 μm^2) since it is implemented on a silicon chip and has the extra advantage of generating an optical comb without an external local oscillator, which reduces its power requirements (under 1 mW) while providing a phase noise of -38.3 dBc/Hz at 1 kHz offset and -97.1 dBc/Hz at 100 kHz offset. The polarization stability and jitter of both implementations are also evaluated. The experimental demonstration evaluates the error vector magnitude (EVM) of frequency-converted 3GPP 5G NR signals using both implementations, confirming the successful transmission with EVM smaller than 12.01% for DD-MZM up to the third harmonic and EVM smaller than 17.36% with the OMCC first harmonic.**

***Index Terms*—Microwave photonics, signal frequency conversion, optomechanical cavities, 5G communications, optical frequency comb, dual-driven Mach-Zehnder modulator.**

Received 12 December 2024; accepted 11 January 2025. Date of publication 20 January 2025; date of current version 4 February 2025. The work of Vicente Fito was supported by UPV under Grant PAID-01-20. The work of Raúl Ortiz was supported by GVA under Grant CIACIF/2021/006. The work of Laura Mercadé was supported in part by Generalitat Valenciana under Grant CIGE/2023/126 and in part by UPV under Grant PAID-06-22. This work was supported in part by Generalitat Valenciana under Grant CIAICO/2021/201 TERAFLEX project and Grant IDIFEDER/2021/061, in part by the Spanish Ministry of Science and Innovation under Grant iPHOEBE PID2023-152410OB-I00, Grant ALLEGRO PID2021-124618NB-C21, and Grant MUSICIAN CHISTERA IV Cofund 2021, and in part by the European Commission under Grant MAGNIFIC HORIZON-CL4-2022-RESILIENCE-01-10 101091968. Funding for open access charge provided by Universitat Politècnica de València. *(Corresponding author: Vicente Fito.)*

The authors are with the Nanophotonics Technology Center, Universitat Politècnica de València, 46022 Valencia, Spain (e-mail: vfitest@ntc.upv.es; rortfer@ntc.upv.es; mmorant@ntc.upv.es; laumermo@ntc.upv.es; amartinez@ntc.upv.es; rllorent@ntc.upv.es).

Digital Object Identifier 10.1109/JPHOT.2025.3532177

I. Introduction

THE relentless growth in data traffic is pushing telecommunication equipment vendors and operators to develop new, more performant and efficient cellular technologies to address new communications paradigms. In particular, 5G-Advanced cellular radio (also known as 5.5G) is an evolutionary step in 5G technology recently released in [1]. 5G-Advanced systems are based on multi-antenna and multi-band operation, targeting the provision of 10 Gbit/s bitrate per user in outdoor, and also indoor scenarios employing seamless multiband operation at sub-6 GHz and millimeter-wave (mm-wave) radio bands [1], [2], [3]. In addition, 3GPP has included in Release 18 new capabilities to generate data-driven network solutions, mainly introducing artificial intelligence and machine learning [4], paving the way to the next release and the 6G era [5]. 5G networks have driven the need for efficient and high-performance frequency conversion techniques to share and maximize the usage of the available RF spectrum. All-optical frequency conversion is particularly advantageous in 5G and next 6G cellular radio systems as it permits multiband frequency conversion to the mm-wave, and efficient operation as the radio signals can be centrally generated and frequency-converted to the desired bands. All-optical frequency conversion gives flexibility due to the feasible high-speed reconfiguration in broad bands and large radio signal bandwidth compared to electronic alternatives [6], [7]. The performance of these systems is significantly influenced by the quality and stability of the RF tone employed in the frequency conversion process [8]. Fig. 1 represents the spectrum of different regulated frequency bands. 5G-Advanced employs 5G signals transmitted in FR1 and FR2 regulated bands for compatibility, as the technology is currently under 3GPP specification [9]. The frequency region FR2 includes the mm-wave Ka and Q bands. 5G FR1 includes the low-frequency L, S and C bands (below 6 GHz) as previous mobile communication technologies (3G and 4G) due

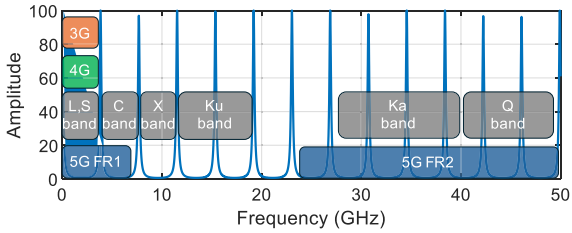

Fig. 1. Example of resulting RF spectrum generated with an optical comb within current regulated frequency bands.

to its characteristics enabling non-line-of-sight (NLOS) communication thanks to combinations of reflected paths, scattering or diffraction. In this application, the implementation of combs presents an attractive solution, for an optical comb generates several RF tones with a constant separation between them, allowing one comb to perform all-optical frequency conversion in a broad range of frequencies. Fig. 1 represents an example of the RF comb spectrum, confirming how different lines of the comb can be used to change from one frequency band to another. The frequency comb consists of a spectrum of discrete, equally spaced and coherent frequency lines. Optical frequency combs are used in various advanced applications, including high-precision metrology, spectroscopy, and telecommunications [10]. The effectiveness of all-optical frequency conversion for radio signals depends on the stability of the frequency drift, phase noise, and power distribution across the comb lines [11], [12]. High-quality microwave sources with ultranarrow linewidths are essential for numerous applications [13]. Oscillators are devices that create a periodic signal (typically a sine wave), showing a narrow tone at a specific frequency.

In the case of microwave oscillators, at frequencies among 0.3–300 GHz, the driving mechanisms can span among opto-electronic oscillators (OEO) and optomechanical oscillators (OMO). The formers can generate high-frequency RF signals with exceptional purity (or extremely narrow linewidth) and good frequency stability performance [14], [15]. One example is based on micro-electro-mechanical systems (MEMS) oscillators which replace traditional quartz crystal oscillators and are built using semiconductor manufacturing techniques [16]. MEMS OEOs consist of a tiny mechanical resonator (whose dimensions are on the micrometer scale) that vibrates at a specific frequency when electrically stimulated, producing a stable and accurate clock signal. Recent studies have also proven that the implementation of silicon nitride microrings to generate optical frequency combs can generate RF microwave tones with a reduced phase noise lower than -96 dBc/Hz at 100 Hz offset, outperforming other studied techniques [17]. However, these systems require a high input power (over 100 mW), with a low coupling efficiency of 30%. A more detailed review of different kinds of opto-electronic oscillators and their key characteristics can be found in recent publications [18]. Conversely, an OMO is a device designed to generate a stable frequency signal through the optomechanical interaction. These oscillators simultaneously support optical and mechanical modes [19]. When optically pumped, the radiation-pressure force excites the mechanical mode within the cavity, leading to coherent oscillations of both the optical and mechanical modes. This process results in a lasing regime, producing a stable frequency comb with several harmonics that are local oscillators. One example resides in cascaded Brillouin scattering within a high-Q silica wedge cavity which enabled the generation of a 21 GHz microwave tone with low phase noise of -160 dBc/Hz [20].

Table I provides a comprehensive comparison of state-of-the-art microwave optical combs generated using different devices and architectures. The columns detail the type of structure, the frequency of the generated microwave tones, the phase noise at 1 kHz and 100 kHz offsets, the equivalent phase noise at a 100 kHz offset scaled to a 5 GHz tone (calculated to standardize the comparison across devices), the power required for operation and the footprint of the device. To ensure a fair comparison, the data presented reflects the performance of each comb in a free-running configuration, preventing the inclusion of additional elements in the setup that could artificially enhance the phase noise performance. In addition, it is worth noting that the ring resonators detailed in [23] employ a MEMS-based design, where the reported phase noise values include the effects of an integrated phase shifter used to enhance the performance. As a result, the footprint of this system accounts for the phase shifter physical dimension, increasing the overall size of the device. The silicon OMCC-based comb implementation evaluated in this work was firstly proposed in [24].

The setup described in [26] uses two separate lasers to generate the optical frequency comb. This configuration underestimates the true footprint of the system, as the reported size does not account for the additional space required to house the second laser. Such discrepancies highlight the importance of considering the complete design of the system when evaluating device performance metrics.

The last four entries of Table I correspond to optical combs generated using MZM. The case reported in [28] corresponds to an indium phosphide (InP) monolithically integrated OFC source based on a DD-MZM. Reference [29] also refers to a photonic integrated structure based on lithium niobite on insulator that uses standard MZM and a phase modulator. A DD-MZM implementation using a feedback loop [30] can enhance the performance.

The values of the DD-MZM comb developed in this work are shown in the last entry of Table I. We can observe that the best phase noise performance of the MZM-based cases corresponds to an implementation using a standard MZM and a phase modulator [29] with a phase noise equivalent of -125 dBc/Hz. However, it requires 380 mW power, a higher power level than the DD-MZM comb herein presented, and it also requires two devices. The proposed DD-MZM provides the second best performance with a phase noise equivalent at 5 GHz of -106 dBc/Hz. The cases just mentioned clearly outperform [28] and [30], which reported phase noise equivalents of -90 dBc/Hz and -87 dBc/Hz with no considerable required power reduction (where [28] does not report required power and [30] only requires 20 mW less than the comb presented in this work but with higher phase noise).

Considering the performance summarized in Table I, the herein proposed OMCC exhibits the lowest footprint (182 μm^2)

TABLE I
COMPARISON OF STATE-OF-THE-ART MICROWAVE OPTICAL COMBS

Optical comb structure and state-of-the-art references	Frequency (GHz)	Phase Noise at 1 kHz (dBc/Hz)	Phase Noise at 100 kHz (dBc/Hz)	Equivalent Phase Noise at 5 GHz (dBc/Hz)	Required Power	Footprint
Slot OMCC [21]	0.113	~ -100	~ -130	-97	400 μW	$\sim 0.36\,\mathrm{mm}^2$
OEO [22]	8.87	~ -55	~ -80	-85	—	$\sim 24\,\mathrm{mm}^2$
Ring resonators [23]	2.05	—	-100	-92	32 mW	$\sim 0.019\,\mathrm{mm}^2$
This work suspended OMCC [24]	3.8	-38.3	-97.1	-95	< 1 mW	$\sim 182\,\mu\mathrm{m}^2$
Photonic integrated microresonator [25]	9.78	~ -50	~ -125	-130	98 mW	$25\,\mathrm{mm}^2$
Photonic integrated ring microresonator [26]	100	~ -50	~ -100	-126	—	$0.16\,\mathrm{mm}^2$
Photonic integrated ring microresonator [27]	227	~ -20	~ -100	-133	370 mW	$\sim 0.031\,\mathrm{mm}^2$
InP DD-MZM [28]	2.8	~ -80	~ -95	-90	—	$\sim 11.25\,\mathrm{mm}^2$
LNOI MZM [29]	5	~ -118	~ -125	-125	380 mW	—
Self oscillating DD-MZM [30]	11.84	~ -85	~ -80	-87	20 mW	—
This work DD-MZM	3.8-13	-88.5	-108.3	-106	40 mW	—

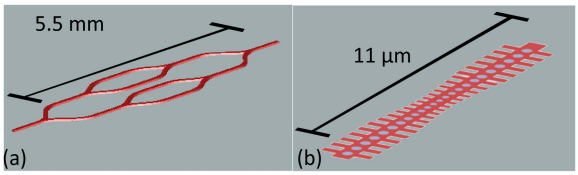

Fig. 2. Visual representation and length examples of the device structures: (a) DD-MZM and (b) silicon OMCC.

and the second-lowest power requirement, while maintaining average phase noise performance. Other combs that achieve a significant reduction in phase noise exhibit a substantial increase in power consumption (by a factor of 100) and a notable expansion in footprint (from $\sim 182\,\mu\mathrm{m}^2$ to $\sim 0.031\,\mathrm{mm}^2$) compared to the suspended OMCC proposed.

Previous studies have proven the capability of OMO based optical combs to perform all-optical frequency conversion of 3GPP 5G NR signals fulfilling standard requirements [24], while this current study will focus on the comparison employing different optical combs. In this paper, we evaluate experimentally the performance frequency conversion of 5G NR signals using two types of frequency combs: one based on a dual-driven Mach-Zehnder modulator (DD-MZM), as shown in Fig. 2(a), and another based on an optomechanical crystal cavity (OMCC), as depicted in Fig. 2(b). On the one hand, an optical comb can be generated using a DD-MZM driven by two sinusoidal RF signals –coming from the same local oscillator (LO)– with slightly different amplitudes [31]. A continuous-wave (CW) light is modulated with these signals, which produces multiple side-bands with even spectral spacing on both sides of the fundamental component. The spectral spacing is directly related to the RF frequency of LO [32], which provides flexibility to tune the line spacing of the comb with the cost of requiring an external LO. The DD-MZM implementation is suitable for integration with the existing telecommunication infrastructure and adaptable to various application requirements [33], [34].

On the other hand, an optical comb can be obtained using an OMCC taking advantage of the phonon lasing regime. This implementation has the advantage of not requiring an external LO, with the cost of having a fixed line spacing. [35]. The OMCC compactness makes it ideal for applications where space and energy efficiency are critical.

In this work, we evaluate experimentally the error vector magnitude (EVM) of the frequency conversion using these two techniques for comb generation with full-standard 3GPP 5G NR signals, taking into account the phase noise characteristics of the resulting RF tones [36]. This comparison will provide insight into the suitability of each type of comb for specific frequency conversion tasks in 5G networks. The findings from this study will offer valuable guidelines for optimizing all-optical frequency conversion systems to meet the stringent performance requirements of next-generation optical communication networks. A significant aspect of this research involves exploring the performance of the DD-MZM based comb under different spacing conditions. By altering the comb line spacing, we can assess how this flexibility impacts the EVM and phase noise, providing deeper insights into optimizing the comb for specific frequency conversion tasks in 5G networks.

This paper is structured as follows: In Section II, the experimental setups used to generate the frequency combs and to evaluate their performance for frequency conversion are presented. The polarization stability is evaluated for both comb implementations. In Section III, the performance of the all-optical frequency conversion of 5G NR signals using the different harmonics of the frequency combs is evaluated in both up- and down-conversion processes, taking into account the signal to noise ratio (SNR) of the resulting frequency-converted 5G NR signals. In addition, the phase noise level, frequency drift and jitter are evaluated for both comb generation techniques. In Section IV, the flexibility of the frequency comb for different carrier separations is evaluated experimentally in terms of EVM and phase noise. Finally, in Section V, the main conclusions of this work are highlighted, presenting the advantages of weaknesses of both comb generation techniques for their application to 5G and beyond-5G systems.

II. EXPERIMENTAL SETUPS FOR COMB GENERATION AND FREQUENCY CONVERSION

Fig. 3 illustrates the experimental setups employed for the all-optical frequency conversion of 3GPP 5G NR signals employing two different optical comb implementations: one based on a DD-MZM and the other on an OMCC. Both combs are generated with a carrier separation of $f_{LO} = 3.84$ GHz, corresponding to the mechanical resonance frequency of the OMCC.

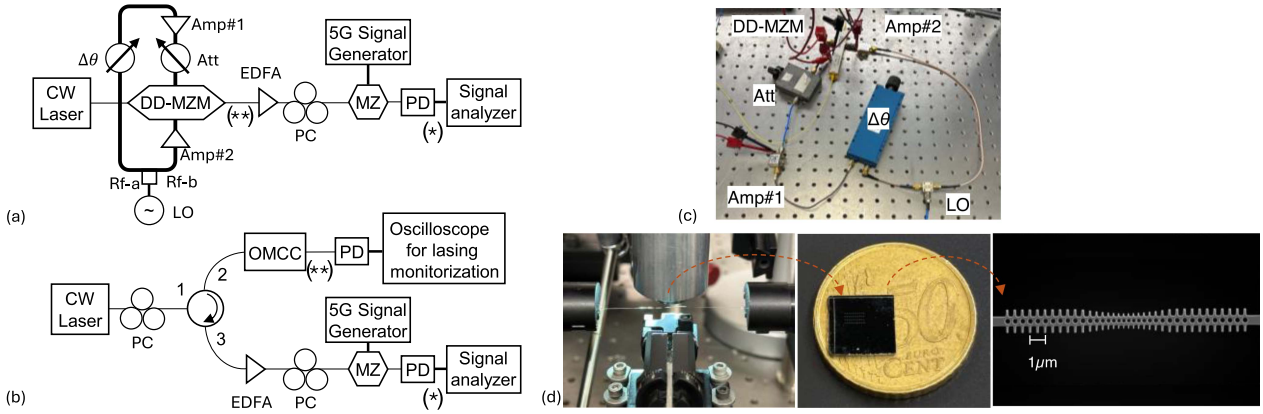

Fig. 3. Experimental setup for comb generation and all-optical frequency conversion using a: (a) DD-MZM and (b) OMCC. Measurement point (*) at which the EVM, phase noise and electrical spectrums were obtained and (**) where the polarization stability is evaluated. Photographs of the key elements of the laboratory testbed: (c) DD-MZM based comb and (d) suspended OMCC and fiber loop, comparison of the silicon chip containing multiple OMCCs with a fifty-cents coin and a SEM image of the OMCC evaluated in this work.

For a fair comparison, both setups employ the same CW laser, Erbium-doped fiber amplifier (EDFA) and 5G signal generation and reception devices. The data signal follows the 3GPP 5G NR standard and is generated with R&S SMW200A at $f_0 = 1$ GHz center frequency for up-conversion and at $f_0 = 8.68$ GHz for down-conversion. The study is performed with various electrical bandwidths (BWs) spanning the complete 3GPP 5G NR specification range, from 5 MHz to 100 MHz. To maintain a consistent SNR, the electrical power level of the generator is adjusted accordingly for each BW. The 5G NR signal is modulated using a Mach-Zehnder modulator operating at the quadrature bias (QB) point. The received optical signal is received by a 40-GHz BW photodetector (PD), model XPDV2120RA, and the frequency-converted signals corresponding to each harmonic (k) of the comb are analyzed using a signal and spectrum analyzer (R&S FSW43).

On one hand, Fig. 3(a) shows the DD-MZM based setup, where an electrical LO at f_{LO} is split into two branches (namely Rf-a and Rf-b). Signal in Rf-a undergoes phase shifting ($\Delta\theta$) and attenuation (Att) to achieve a spectrally flat comb with a tolerance of ± 2.5 dB. The DD-MZM comb implementation allows tuning the carrier separation by modifying the value of f_{LO}. In first place we compare the performance with the carrier same separation at $f_{LO} = 3.84$ GHz. Different separations are evaluated in Section IV.

On the other hand, Fig. 3(b) depicts the OMCC-based setup. Optomechanical interaction in OMCCs is mediated by the radiation-pressure force, enabling the exchange of energy and momentum between photons and phonons. A dynamical backaction between the optical and mechanical modes takes place due to the delayed nature of radiation-pressure force [37], resulting in the optical spring effect, cooling (heating) the OM cavity when the driving laser is red (blue) detuned with respect to the optical resonance [38], [39]. When blue detuned, the cavity can enter into a dynamics in which the optical mode interacts with the mechanical motion reducing its damping rate, leading to a regime of self-sustained oscillations which effectively generates mechanical phonon-based lasing. An optical circulator is used to monitor the optical resonance of the OMCC (at $f_{LO} = 3.84$ GHz) via the transmitted signal, while the reflected signal is used for 5G data modulation and frequency-conversion analysis.

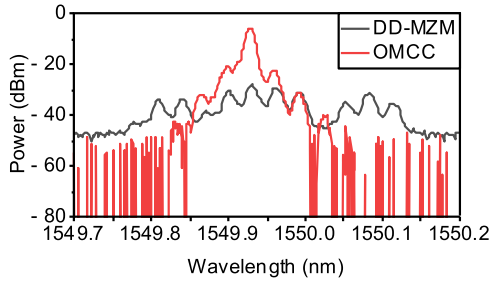

Fig. 4. Measured optical spectrum of the frequency combs generated using DD-MZM and OMCC implementations (RBW= 0.01 nm).

Fig. 4 shows the resulting optical spectra of both comb implementations. The DD-MZM based comb provides a flat amplitude spectrum, whereas the OMCC based comb resembles a step pyramid. The OMCC based comb central wavelength varies from 1520 nm to 1560 nm each time it enters the phonon lasing regime. It can be observed in Fig. 4 that both combs have the same carrier separation of $f_{LO} = 3.84$ GHz sharing a similar central wavelength around 1549.92 nm.

In Fig. 5 the resulting electrical spectra can be analyzed for both comb implementations measured at point (*) of Fig. 3. The DD-MZM comb implementation of Fig. 5(a) shows 10 harmonics with the same separation of $f_{LO} = 3.84$ GHz in the 40 GHz spectrum range, with a power difference between the first and the tenth harmonic of 16.8 dB. Fig. 5(b) shows a power decrease in the higher harmonics of the OMCC-based comb, being the sixth harmonic the highest harmonic that can be distinguished. The power difference between the first and the sixth harmonic in Fig. 5(b) is of 63.6 dB. This power difference will limit the capability to achieve all-optical frequency conversion for higher harmonic orders.

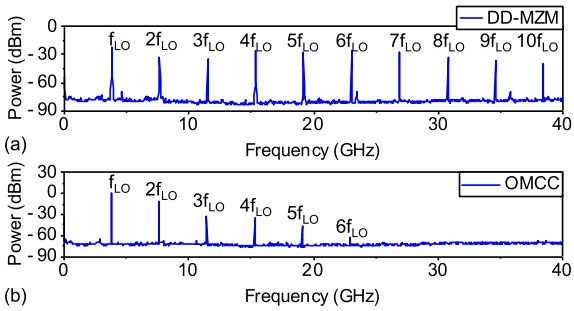

Fig. 5. Measured electrical spectra of the optical frequency combs generated using a: (a) DD-MZM and (b) OMCC (measured with RBW= 1 MHz).

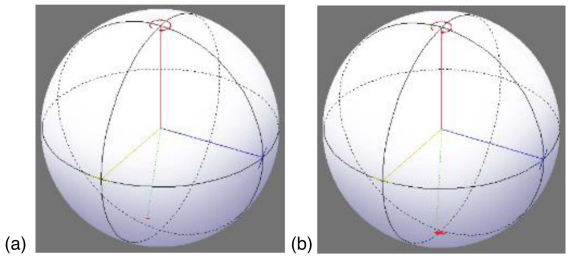

Comb implementation	1 min	5 min	10 min
DD-MZM	0.0020	0.0032	0.0037
OMCC	0.0205	0.0233	0.0858

Fig. 6. Polarization stability represented over the Poincaré sphere measured in a 10-minute interval with 2400 samples at the comb output implemented with: (a) DD-MZM and (b) OMCC. Table with mean deviation from the centroid point from the Stokes vector points calculated for 1-min, 5-min and 10-min intervals for both comb implementations.

The polarization stability at the output of both comb implementations was measured experimentally at point (**) of Fig. 3 with Optellios PS2000 polarization analyzer. The stability is measured over 1- and 5-minute intervals with steps of 10 ms and a 10-minute interval with steps of 250 ms. The polarization at the output of the optical combs is represented in the Poincaré sphere for the 10-minute interval for both DD-MZM –Fig. 6(a)– and OMCC implementations –Fig. 6(b)–. The Stokes parameters S1, S2 and S3 are measured and, for each time interval and implementation, we calculated the centroid and the respective deviation of the clustered points of the dataset. The calculated mean deviation is also included in Fig. 6. The experimental results confirm that the DD-MZM implementation is more stable in polarization, achieving one order of magnitude less than the mean deviation provided by the OMCC output. However, both implementations are very stable, as it can be confirmed in the small variation reported in both Poincaré spheres of Fig. 6.

III. Performance Comparison for Frequency Conversion

A. Up-Conversion EVM Performance

In this subsection, the resulting electric spectra and the EVM of the upconverted signals are evaluated in detail using both OMCC and DD-MZM comb implementations. The analyzed frequency-converted 5G signals are highlighted with red boxes

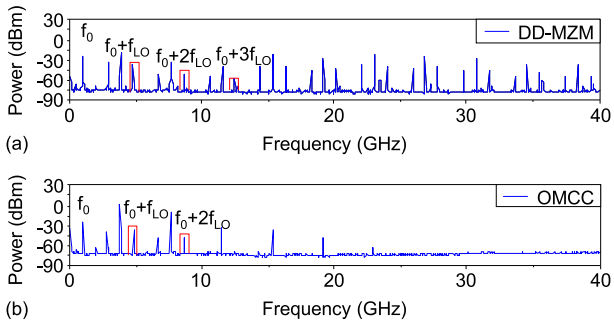

Fig. 7. Resulting electrical spectra of the optical frequency combs generated using a: (a) DD-MZM and (b) OMCC including the up-converted 5G signals (measured with RBW= 1 MHz).

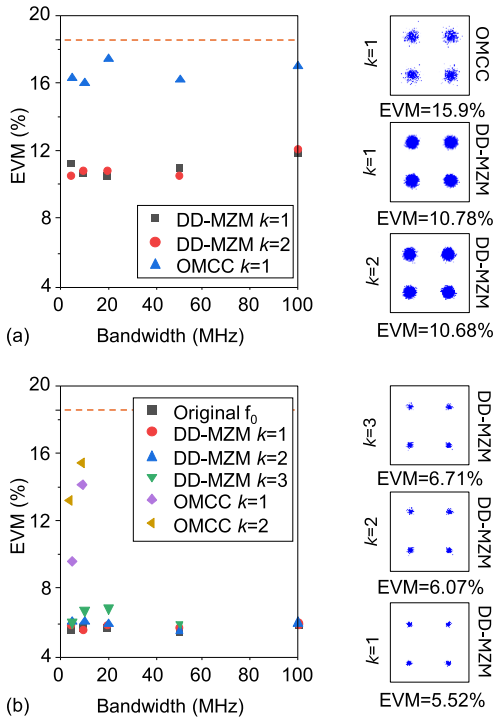

Fig. 8. Measured EVM and constellations of the PDSCH upconverted signals at $kf_m + f_0$ vs. BW, measured with constant SNR: (a) SNR = 19.5 dB and (b) SNR = 25 dB. 3GPP 5G NR EVM recommendation included as a horizontal dashed line.

in the received electrical spectra shown in Fig. 7. The original 5G signal is generated at f_0 =1 GHz and the upconverted replicas can be found at linear combinations of f_0 and each comb harmonic k as $|f_0 \pm k \cdot f_{LO}|$. Using the first harmonic ($k = 1$), we obtain two replicas centered at $f_{LO} \pm f_0$. With the second harmonic ($k = 2$), the replicas appear at $2f_{LO} \pm f_0$. For the third harmonic ($k = 3$), the replicas appear at $3f_{LO} \pm f_0$. In these experiments, we evaluate the worst-case scenario, corresponding to the higher frequency replicas. Specifically, using the first harmonic, we evaluate the 5G signal upconverted to $f_{LO} + f_0 = 4.84$ GHz, corresponding to the regulated 5G band n79, while the upconverted signals using the second and third harmonic lie in the X and Ku bands, as depicted previously in Fig. 1.

Fig. 8 shows the EVM performance of the upconverted signal using different harmonics for each comb implementation, compared with the 3GPP standard EVM recommendation for 5G NR physical data shared channels (PDSCH) modulated with QPSK of 18.5%[40], included as reference as a horizontal dashed line. For a fair comparison, the EVM vs. bandwidth performance is evaluated with two different constant SNR levels of 19.5 dB in Fig. 8(a) and 25.0 dB in Fig. 8(b), respectively. Fig. 8 insets show the received constellations for 10 MHz BW signals for different cases. It can be observed in Fig. 8(a) that the EVM of the upconverted 5G signals using the DD-MZM comb shows a nearly constant behavior with all EVM values ranging from 10% to 12% (with a maximum variation under 1% between contiguous measures) for both harmonics ($k = 1$ and $k = 2$). Up-conversion using the OMCC comb exhibits higher EVM values and variation for the same SNR level, obtaining EVM in the range from 15.9% to 17.5% for $k = 1$, being this maximum variation between contiguous measures. The higher SNR evaluated in Fig. 8(b) permits to extend the analysis to higher order harmonics, studying also the performance using the second harmonic $k = 2$ of the OMCC comb implementation and the third harmonic $k = 3$ of the DD-MZM implementation. The EVM performance of original signal at $f_0 = 1$ GHz is also included in Fig. 8(b) to confirm that the EVM barely degrades when upconverting the signals using the DD-MZM based comb. The EVM values of the original $f_0 = 1$ GHz are located in the range between 5.40% and 5.89%. All the up-converted EVM values up to 100 MHz BW using the DD-MZM implementation are between 5.52% and 6.84%, with a maximum variation under 1% between contiguous measures for the third harmonic and under 0.5% for lower-order harmonics. As it can be observed also in the received spectra included in Fig. 7, the higher-order harmonics of the OMCC-based comb have a significant power reduction, and for this reason the upconverted replica using the second harmonic requires a higher electrical power level. This limits the operation of the OMCC-based comb for up-conversion using the second harmonic to signal bandwidths of 10 MHz or lower, as the results obtained show a high variability in EVM (increasing up to 5% between contiguous measures). The EVM of the 5G signals upconverted with $k = 1$ are in the range from 9.62% to 14.15%, whereas for signals upconverted with $k = 2$ this range is from 13.22% to 15.38%. We can confirm in the spectrum of Fig. 7(a) that this limitation is not present in DD-MZM comb generation, where all the generated harmonics and the resulting replicas mantain a similar level.

B. Down-Conversion EVM Performance

Fig. 9 presents the received spectra and EVM performance results for down-conversion of 5G signals using both comb implementations. In this case, for down-conversion, the central frequency of the original signal was established at $f_0 = 8.686$ GHz, so the up- and down-converted replicas using the first harmonic are generated at the same frequency $f_{up} + f_{LO} = f_{down} - f_{LO} = 4.84$ GHz, for a fair comparison. Fig. 9(a) and (b) present the electrical spectra for down-conversion using the DD-MZM and the OMCC implementations, where

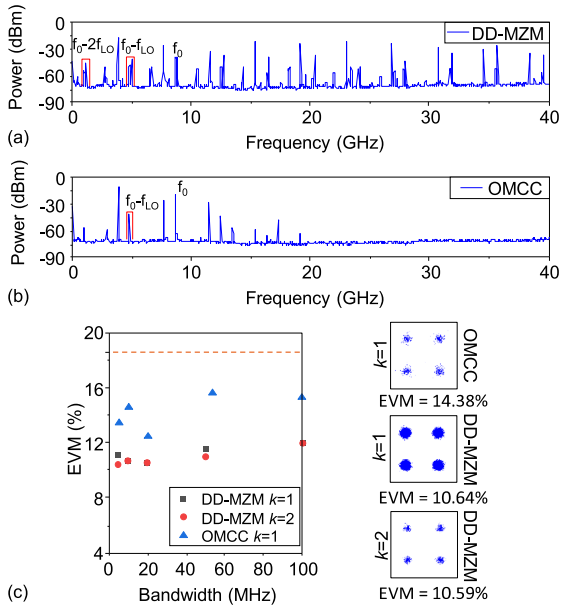

Fig. 9. Resulting electrical spectra of the frequency combs generated using a: (a) DD-MZM and (b) OMCC including the down-converted 5G signals (measured with RBW= 1 MHz). (c) Received EVM for constant SNR = 19.5 dB and constellations of the PDSCH upconverted signals at $kf_m + f_0$ vs. BW. 3GPP 5G NR EVM recommendation included as a horizontal dashed line.

the analyzed frequency bands are highlighted with red boxes. As in the previous subsection, we can appreciate that with the DD-MZM implementation, the different harmonics maintain a similar power level. On the other hand, the OMCC based comb only generates six harmonics, with the power of each harmonic decreasing as the harmonic order increases. Fig. 9(c) shows the EVM performance of the downconverted signals across the complete range of 3GPP 5G NR specification BWs (from 5 MHz to 100 MHz). In order to be able to compare also with the upconversion process shown in Fig. 8(a), these measures are taken with a constant SNR level of 19.5 dB. The EVM values in down-conversion using the DD-MZM comb are in the range from 10.42% to under 11.96%, with a maximum variation between contiguous measures of 1.08%. The EVM values in down-conversion using the OMCC-based comb lie between 12.44% and 15.58% (with this variation occurring between contiguous measures). It can be observed that the behavior is similar in both up- and down-conversion processes, where there is an increase in EVM and variability using the OMCC implementation while there is no distinguishable difference between the first and second harmonics of the DD-MZM.

C. Phase Noise and Frequency Drift Evaluation

Fig. 10(a) reports the phase noise levels at different frequency offsets for the different harmonics employed in the up- and down-conversion processes. We can observe an increase of phase noise level for low frequency offsets when comparing the OMCC and the DD-MZM implementations. For offsets lower than 1 kHz, there is a constant increase in phase noise in the OMCC-based comb over 50.8 dB. For offsets over 1 MHz the phase noise levels for both comb implementations reach similar

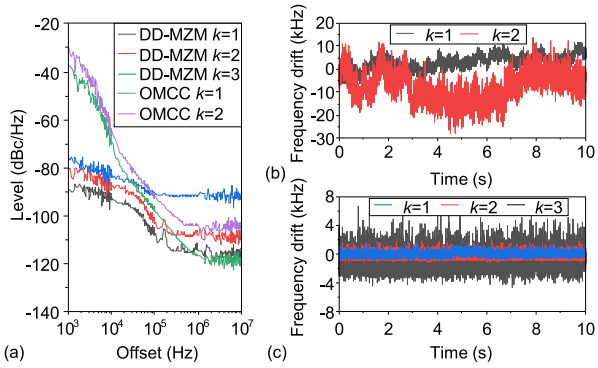

Fig. 10. (a) Phase noise measured for the different harmonics of comb generated with both OMCC and DD-MZM implementations where k denotes the harmonic order. Frequency drift of the k-th harmonic (measured over 10 s) when generated with: (b) OMCC and (c) DD-MZM.

values, with a deviation under 4.85 dB when comparing the same harmonic. If we compare the performance of different harmonics generated with the same comb implementation, it can be seen that the phase noise increases with the harmonic order. In the case of the DD-MZM based comb, for offsets lower than 10 kHz, phase noise increases 6.19 dB as a maximum for each increase in harmonic order. For offsets over 100 kHz, the variation between the first and second harmonic is 6.84 dB, whereas for the third harmonic the phase noise increases up to 16.37 dB. Fig. 10(b) and (c) show the frequency drift measured of the harmonics generated with both implementations over 10 seconds. In both cases, it can be observed that the frequency drift increases as the harmonic order increases, with the lowest harmonic offering the lowest frequency drift in each comb implementation. However, the differences in scales between Fig. 10(b) and (c) are also noticeable, where the scale range for the DD-MZM based comb is of 16 kHz, while the scale range for the OMCC-based comb covers 50 kHz. The frequency drift for the second harmonic ($k = 2$) of the OMCC-based comb is measured as 41.627 kHz, which is over double of the first harmonic ($k = 1$) of 18.481 kHz. In the case of the DD-MZM based comb, the maximum frequency drift corresponding to the third harmonic ($k = 3$) is 11.188 kHz the maximum frequency drift for the second harmonic ($k = 2$) is 3.172 kHz and the maximum frequency drift measured for the first harmonic ($k = 1$) is of 2.352 kHz.

The jitter of the different RF tones generated by both optical frequency combs has also been evaluated, integrating the phase noise of the different RF tones from 10 kHz to 100 kHz. The jitter values for the OMCC-based comb are 1.1825 ps for the first harmonic and 1.1036 ps for the second harmonic. In the case of the DD-MZM based comb, the jitter values calculated for the different harmonics are reduced to 0.2004 ps for the first harmonic, 0.1984 ps for the second harmonic and 0.2468 ps for the third harmonic. It can be noted that, in the case of the OMCC-based comb, the second harmonic offers lower jitter values than the first harmonic. Thus, there is no clear relationship between harmonic order and jitter. Although frequency drift increases with the harmonic order, the definition of jitter compensates this effect. Since the phase noise integral is divided by the central frequency of the generated RF tone, the impact of phase noise is mitigated, resulting in stable jitter across the studied ranges.

Taking into account the results presented in Fig. 10, the increased dispersion in the measured EVM using the OMCC-based comb can be explained due to the increase of the harmonic's frequency drift. The central frequency of the OMCC resonance is constantly shifting, causing the central frequency of the frequency-converted signal to shift as well. This shift in central frequency results in a frequency mismatch between the central frequency of the upconverted signal and the demodulator. In particular, the signal analyzer used in these experiments (R&S FSW43) can demodulate the 5G NR signal with frequency mismatches up to 8 kHz, whereas in Fig. 10, frequency drifts higher than 10 kHz are observed using the first harmonic of the OMCC ($k = 1$). Depending on when the upconverted signal is captured, this mismatch is randomly assigned, leading to higher variability in the received EVM. Up-conversion using the second harmonic of the OMCC ($k = 2$) shows a considerable increase in EVM value and its variation. Furthermore, the increase in EVM values for frequency conversions using the OMCC-based comb, compared to the DD-MZM-based comb, coincides with the higher phase noise at low frequency offsets of the OMCC-based comb.

IV. Performance With Different Carrier Separation

A. Up-Conversion Performance to Different Frequency Bands

We extended the evaluation of the frequency conversion to different frequency bands by using different carrier separation of the comb. This is possible using the DD-MZM implementation by changing the f_{LO}, but could be also possible by designing the OMCC with a different mechanical frequency [22]. As mentioned before, one of the key advantages of using a DD-MZM based comb is that it offers the possibility of tuning the carrier separation by adjusting f_{LO} [34], at the cost of needing an external oscillator.

Following the different frequency regions available in the range up to 50 GHz depicted previously in Fig. 1, we evaluate different comb carrier separation (f_{LO}) ranging from 3.84 GHz to 13 GHz. In particular, using a carrier separation of 13 GHz and a central frequency of the 5G signal of $f_0 = 15$ GHz, the up-converted replicas are generated at 2 GHz, 28 GHz and 41 GHz, corresponding to 3GPP 5G NR regulated frequency bands n70, n257 and n259, respectively. In addition, the $f_{LO} = 3.84$ GHz used in the previous section lies directly in band n77 (from 3300 MHz to 4200 MHz), which is a band extensively used in Europe [41], enabling its frequency conversion between the n77 band and low frequency signals ($f_0 < 0.3$ GHz).

Fig. 11(a) shows the resulting electrical spectra of the DD-MZM comb implementation using different f_{LO}. The noise level keeps almost constant for different carrier separation, confirming that it is independent from the f_{LO}. The EVM performance of the up-conversion process with different SNR levels (also 19.5 dB and 25 dB for a fair comparison with the previous section) is represented in Fig. 11(b). In this case, the study is limited to the frequency up-conversion using the first harmonic in the DD-MZM implementation ($k = 1$). The original 5G signal is generated with central frequency of 1 GHz and 10 MHz BW. For the SNR = 19.5 dB curve, the EVM values are between 10.4% and 10.8%, whereas for the SNR = 25 dB curve, the

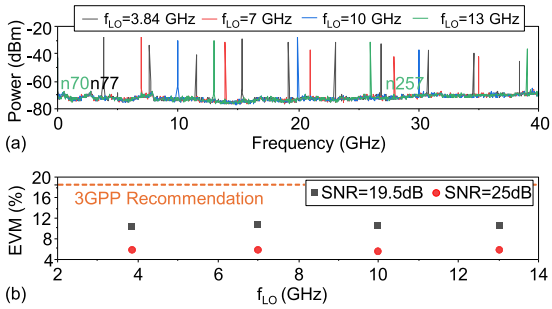

Fig. 11. (a) Measured electrical spectrum of the optical frequency combs generated using a DD-MZM with different f_{LO} including regulated bands n70 (at 2 GHz), n77 (3.7 GHz) and n257 (28 GHz) (measured with RBW= 1 MHz). (b) Measured EVM of 10 MHz 5G upconverted signals for different carrier spacing comb configurations using the first harmonic ($k = 1$) and different SNR.

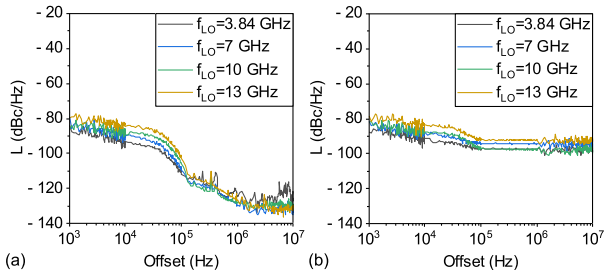

Fig. 12. Phase noise of the: (a) first harmonic and (b) RF tone corresponding to the upconverted signal using the first harmonic of the comb generated with the DD-MZM for different f_{LO}.

EVM values are between 5.5% and 5.9%. These values match with the EVM performance in upconversion using the DD-MZM implementation reported previously in Fig. 8.

B. Phase Noise Evaluation for Different Frequency Bands

Fig. 12(a) shows the phase noise of the harmonic responsible for frequency up-conversion for different carrier separation using the DD-MZM implementation (f_{LO}). In addition, Fig. 12(b) depicts the phase noise curves of an upconverted tone at $f_{LO} + 1$ GHz measured by turning off the modulation of the signal generation and keeping the RF tone from which we can extract the phase noise. While Fig. 12(a) illustrates a sharp decline from -96.05 dB to -86.19 dB, dropping to lower than -116.08 dB, Fig. 12(b) shows no such decrease beyond 100 kHz, maintaining the curves consistently within the -88.56 dB to -101.67 dB range.

If we observe the relationship between the phase noise and the different f_{LO} we can observe that from 10 kHz up to 100 kHz in Fig. 12(a) and up to 1 MHz Fig. 12(b), the variation of each of the curves is much lower, and it allows us to calculate the difference in dB between them. For Fig. 12(a) the maximum variation measured was a 4.08 dB increase in phase noise for each step increasing f_{LO}, whereas for Fig. 12(b) this variation is a 4.78 dB increase as maximum. It should be noted that for Fig. 12(b), in this specified region, the results obtained for an external f_{LO} of 10 GHz overlap for offsets lower than 10 kHz with the results obtained from an external $f_{LO} = 7$ GHz. For offsets higher than 10 kHz, they overlap with the results obtained from an external $f_{LO} = 3.84$ GHz.

V. Conclusion

In this paper, the performance of optical frequency combs generated using DD-MZM and OMCC is evaluated for all-optical frequency conversion of 3GPP 5G NR signals in both up- and down-conversion processes for different harmonic orders. The results revealed significant differences in their capabilities for up-conversion and down-conversion of telecommunication signals such as 5G signals.

The DD-MZM based implementation obtains a broader range of harmonics with consistent power levels up to 40 GHz, maintaining sufficient SNR for effective frequency conversion without deteriorating the frequency-converted signal. In contrast, the OMCC-based comb shows a decrease in power for higher harmonics, which limits the performance of frequency-conversion for higher frequency bands. The OMCC-based comb's highest order harmonic detected corresponded to a frequency of 23.04 GHz. In terms of polarization, both implementations are stable at the comb output, although the DD-MZM based comb has an order of magnitude less deviation from the centroid point defined by the Stokes parameters in a 10-minute interval. And in terms of EVM performance, the DD-MZM based comb provides stable EVM values across higher-order harmonics and different SNR levels, with minimal variation between measures, highlighting a very slight EVM degradation when the harmonic order is increased. Within the same harmonic and the same SNR level, the maximum EVM variation measured was 1.54%. Conversely, the OMCC-based comb shows a higher and more variable EVM (the maximum variation measured was over 5%) due to increased phase noise and frequency drift of the carrier used for the frequency-conversion. When comparing the first harmonic of both comb implementations, at low frequency offsets ($<$1 kHz) the phase noise level of the OMCC based comb is at least 50.8 dB higher than the DD-MZM-based comb implementation. The frequency drift in this case is measured over 18 kHz for the OMCC, whereas for the DD-MZM the measured frequency drift is under 3 kHz. This variability limits the OMCC-based comb application to frequency upconversion using the second harmonic ($k = 2$), meeting the 3GPP recommendation with 5G signals with bandwidths equal or lower than 10 MHz.

Similar trends are observed in the down-conversion process, where the DD-MZM comb implementation maintains low and stable EVM values (ranged from 10.42% to 11.96% in all the 3GPP BW range from 5 to 100 MHz), while the OMCC implementation exhibits higher EVM values and greater variability (ranged from 12.44% to 15.58%).

The flexibility of the DD-MZM implementation in tuning the carrier separation of the comb was also evaluated experimentally by modifying the external f_{LO} to upconvert the 5G signal to different frequency bands, obtaining consistent EVM and phase noise performance across carrier separations up to 13 GHz. This adaptability makes the DD-MZM comb implementation a more flexible and stable solution for all-optical frequency conversion in telecommunications, meeting the stringent requirements of modern 5G networks. Both comb implementations have been

proven to comply with 3GPP 5G NR requirements using the first and second harmonics of the comb, and even though the DD-MZM based comb presents lower phase noise, EVM and frequency drift values, in specific applications the compactness and reduced footprint of the OMCC ($\approx 182\,\mu\mathrm{m}^2$) can provide a better solution. For most cases, the implementation of a DD-MZM-based comb offers many advantages compared to an OMCC-based comb, such as the reduced EVM and phase noise, lower frequency drift, higher polarization stability or the capability of generating more harmonics and reaching higher frequencies. However, in specific cases where size and weight are key parameters to take into account (such as in satellite communications), the implementation of an OMCC-based comb can be preferable as they provide much smaller footprint, reduced weight and most importantly they do not require an external LO signal to generate the comb, which simplifies the overall system while providing an acceptable phase noise. Ongoing work in OMCC-based combs could reduce the phase noise by implementing a closed loop, where the output is fed back into the input to decrease frequency offset and improve the stability of higher-order harmonics.

REFERENCES

[1] GSMA, "5G-Advanced: Shaping the future of operator services marketing paper," Tech. Rep., 2024. [Online]. Available: https://www.gsma.com/solutions-and-impact/technologies/networks/gsma_resources/5g-advanced-shaping-the-future-of-operator-services/#toform

[2] Y. Heng et al., "Six key challenges for beam management in 5.5G and 6G systems," *IEEE Commun. Mag.*, vol. 59, no. 7, pp. 74–79, Jul. 2021.

[3] Huawei, "5G-Advanced technology evolution from a network perspective," Tech. Rep., 2021. [Online]. Available: https://www-file.huawei.com/-/media/CORP2020/pdf/event/1/5G_Advanced_Technology_Evolution_from_a_Network_Perspective_2021_en.pdf

[4] X. Lin, "An overview of 5G advanced evolution in 3GPP release 18," *IEEE Commun. Standards Mag.*, vol. 6, no. 3, pp. 77–83, Sep. 2022.

[5] A. Toskala and H. Holma, *5G-Advanced Overview*. Hoboken, NJ, USA: Wiley, 2024, ch. 16, pp. 485–503.

[6] E. Stassen et al., "Ultra-low power all-optical wavelength conversion of high-speed data signals in high-confinement AlGaAs-on-insulator microresonators," *Appl. Phys. Lett. Photon.*, vol. 4, no. 10, 2019, Art. no. 100804.

[7] R. Zhuang et al., "Electro-optic frequency combs: Theory, characteristics, and applications," *Laser Photon. Rev.*, vol. 17, no. 6, 2023, Art. no. 2200353.

[8] A. Liu, J. Dai, and K. Xu, "Stable and low-spurs optoelectronic oscillators: A review," *Appl. Sci.*, vol. 10, no. 5, pp. 1367–1385, 2021.

[9] W. Chen et al., "5G-Advanced toward 6G: Past, present, and future," *IEEE J. Sel. Areas Commun.*, vol. 41, no. 6, pp. 1592–1619, Jun. 2023.

[10] H. Hu and L. Oxenløwe, "Chip-based optical frequency combs for high-capacity optical communications," *Nanophotonics*, vol. 10, no. 5, pp. 1367–1385, 2018.

[11] S. Yoo, S. Choi, J. Kim, H. Yoon, Y. Lee, and J. Choi, "A low-integrated-phase-noise 27–30-GHz injection-locked frequency multiplier with an ultra-low-power frequency-tracking loop for mm-wave-band 5G transceivers," *IEEE J. Solid-State Circuits*, vol. 53, no. 2, pp. 375–388, Feb. 2018.

[12] M. A. Ilgaz and B. Batagelj, "Application of an opto-electronic oscillator in 5G mobile and wireless networks with a low frequency drift, a high side-modes-suppression ratio and without a power penalty due to chromatic dispersion," in *Proc. Eur. Conf. Netw. Commun.*, Ljubljana, Slovenia, 2018, pp. 388–392.

[13] I. Kudelin et al., "Photonic chip-based low-noise microwave oscillator," *Nature*, vol. 627, pp. 534–539, 2024.

[14] L. Maleki, "The optoelectronic oscillator," *Nature Photon.*, vol. 5, no. 12, pp. 728–730, 2011.

[15] X. S. Yao and L. Maleki, "Optoelectronic microwave oscillator," *J. Opt. Soc. Amer. B*, vol. 13, no. 8, pp. 1725–1735, 1996.

[16] J. T. M. van Beek and R. Puers, "A review of MEMS oscillators for frequency reference and timing applications," *J. Micromechanics Microeng.*, vol. 22, 2011, Art. no. 013001.

[17] I. Kudelinet al., "Photonic chip-based low-noise microwave oscillator," *Nature*, vol. 327, pp. 534–539, 2024.

[18] T. Hao, W. Li, N. Zhu, and M. Li, "Perspectives on optoelectronic oscillators," *APL Photon.*, vol. 8, no. 2, 2023, Art. no. 020901.

[19] M. Aspelmeyer, T. J. Kippenberg, and F. Marquardt, "Cavity optomechanics," *Rev. Modern Phys.*, vol. 86, no. 4, pp. 1391–1452, 2014.

[20] J. Li, H. Lee, and K. J. Vahala, "Microwave synthesizer using an on-chip Brillouin oscillator," *Nature Commun.*, vol. 4, 2013, Art. no. 2097.

[21] X. Luan et al., "An integrated low phase noise radiation-pressure-driven optomechanical oscillator chipset," *Sci. Rep.*, vol. 4, 2014, Art. no.6842.

[22] J. Tang et al., "Integrated optoelectronic oscillator," *Opt. Exp.*, vol. 26, no. 9, pp. 12257–12265, 2018.

[23] S. Tallur, S. Sridaran, and S. A. Bhave, "A monolithic radiation-pressure driven, low phase noise silicon nitride opto-mechanical oscillator," *Opt. Exp.*, vol. 19, no. 24, pp. 24522–24529, 2011.

[24] V. Fito, R. Ortiz, M. Morant, L. Mercadé, R. Llorente, and A. Martínez, "Experimental evaluation of all-optical up- and down-conversion of 3GPP 5G NR signals using an optomechanical crystal cavity frequency comb," *J. Lightw. Technol.*, vol. 24, no. 19, pp. 6825–6831, Oct. 2024.

[25] J. Liu et al., "Photonic microwave generation in the X- and K-band using integrated soliton microcombs," *Nat. Photon.*, vol. 14, no. 8, pp. 486–491, 2020.

[26] S. Sun et al., "Integrated optical frequency division for microwave and mmwave generation," *Nature*, vol. 627, no. 8004, pp. 540–545, 2024.

[27] Y. Zhao et al., "All-optical frequency division on-chip using a single laser," *Nature*, vol. 627, no. 8004, pp. 546–552, 2024.

[28] E. S. Lima, N. Andriolli, E. Conforti, G. Contestabile, and A. C. S. Junior, "Integrated optical frequency combs for low-phase noise mm-waves generation," in *Proc. 2022 Conf. Lasers Electro- Opt.*, 2022, pp. 1–2.

[29] Y. Zhang et al., "Flat optical frequency comb generation based on monolithic integrated LNOI intensity and phase modulator," *Photonics*, vol. 9, no. 7, 2022, Art. no. 495.

[30] G. K. M. Hasanuzzaman, A. Kanno, P. T. Dat, and S. Iezekiel, "Self-oscillating optical frequency comb: Application to low phase noise millimeter wave generation and radio-over-fiber link," *J. Lightw. Technol.*, vol. 36, no. 19, pp. 4535–4542, Oct. 2018.

[31] T. Sakamoto, T. Kawanashi, and M. Izutsu, "Widely wavelength-tunable ultra-flat frequency comb generation using conventional dual-drive Mach-Zehnder modulator," *Electron. Lett.*, vol. 43, pp. 1039–1040, 2007.

[32] I. Morohashi, T. Sakamoto, H. Sotobayashi, T. Kawanishi, and I. Hosako, "Broadband optical comb generation using Mach-Zehnder-modulator-based flat comb generator with feedback loop," in *Proc. 36th Eur. Conf. Exhib. Opt. Commun.*, 2010, pp. 1–3.

[33] P. Jiang, P. Li, and Y. Fan, "Broadband optical frequency comb generation based on single electro-absorption modulation driven by radio frequency coupled signals," *Front. Optoelectron.*, vol. 15, no. 45, pp. 1–8, 2022.

[34] Y. Liu and S. Wu, "Proposed scheme for ultra-flat optical frequency comb generation based on dual-drive Mach–Zehnder modulators and bidirectional recirculating frequency shifting in single loop," *Photonics*, vol. 9, no. 8, 2022, Art. no. 514.

[35] L. Mercadé, L. L. Martin, A. Griol, D. Navarro-Urrios, and A. Martínez, "Microwave oscillator and frequency comb in a silicon optomechanical cavity with a full phononic bandgap," *Nanophotonics*, vol. 9, no. 11, pp. 3535–3544, 2020.

[36] H. Wang, B. Wu, H. Zhou, W. Wang, and G. Xu, "Optical tunable frequency-doubling OEO using a chirped FBG based on orthogonally polarized double sideband modulation," *Photonics*, vol. 10, no. 9, 2023, Art. no. 1002.

[37] T. Kippenberg and K. Vahala, "Optomechanics: Back-action at the mesoscale," *Science*, vol. 321, no. 5893, pp. 1172–1176, 2008.

[38] R. Ortiz, L. Mercadé, A. Grau, D. Navarro-Urrios, and A. Martínez, "Influence of thermal effects on the optomechanical coupling rate in acousto-optic cavities," *Phys. Rev. A*, vol. 109, no. 2, 2024, Art. no. 023504.

[39] J. Chan et al., "Laser cooling of a nanomechanical oscillator into its quantum ground state," *Nature*, vol. 478, pp. 89–92, 2011.

[40] *3GPP, 5G; NR; Base Station (BS) conformance Testing Part 1: Conducted conformance Testing*, 3GPP Tech. Specification TS 38.141-1 version 15.15.0 release 15, 2023.

[41] A. Zhao and Z. Ren, "Wideband MIMO antenna systems based on coupled-loop antenna for 5G N77/N78/N79 applications in mobile terminals," *IEEE Access*, vol. 7, pp. 93761–93771, 2019.